08

Investigation of the effect of ZnSe evaporation conditions using an ytterbium laser on the production of nanoparticles by this method and on their properties

© V.V. Osipov,[1] V.V. Platonov,[1] V.V. Lisenkov,[1] K.I. Demidova,[1] S.V. Zayats,[1] M.P. Zykova[2]

[1] Institute of Electrophysics, Ural Branch, Russian Academy of Sciences,
620016 Yekaterinburg, Russia
[2] Russian University of Chemistry and Technology named after D.I. Mendeleev,
125047 Moscow, Russia
e-mail: platonov@iep.uran.ru

Received May 12, 2023
Revised July 27, 2023
Accepted July 31, 2023

Using laser evaporation method of a target with followed condensation in a flow of buffer gas (Ar or He) the preparation of ZnSe, Fe:ZnSe, Cu:ZnSe nanopowders and their properties were studied. It is shown that for the same gas pressure (100 kPa), ZnSe nanoparticles obtained in helium have a smaller average size (11 nm), than in argon (18 nm). An increase in Ar pressure from 100 to 300 kPa led to an increase in the size of nanoparticles even further 2 times. The influence of laser radiation parameters and gas parameters on productivity of nanopowders obtaining was studied process. The nanopowders had cubic and hexagonal crystalline ZnSe phases, the content of which varied within certain limits depending on gas parameters. A comparison of theoretical and experimental data suggests that a significant part of nanoparticles were formed by desublimation of vapor directly into the solid phase. The results of the first studies of pressing and sintering of ZnSe nanopowders, obtained by laser method, are shown.

Keywords: Nanopowder, gas-phase method for the synthesis of nanoparticles, laser ablation, zinc selenide, ytterbium fiber laser.

DOI: 10.61011/TP.2023.10.57455.124-23

Introduction

Zinc selenide is a popular and often indispensable optical material for infrared optics elements [1,2]. A significant progress has been made in recent years in its use as a matrix for active elements of solid-state lasers emitting at a wavelength of $\lambda = 3.77-5.05\,\mu$m ($Fe^{2+}:ZnSe$) [3,4] and $\lambda = 1.88-3.10\,\mu$m ($Cr^{2+}:ZnSe$) [5]. The most difficult moment in the creation of such lasers is the technology of manufacturing the moonshine of the active element, in particular, the doping of ZnSe with Fe or Cr ions. Therefore, there is now a great interest in ceramic methods of their creation, including the method of hot pressing [6]. This will make it possible to produce homogeneous elements of large volume, including those with a composite structure. At the same time, it is best to dope zinc selenide with Fe or Cr ions at the powder preparation stage. It is necessary to use high-purity powders containing slightly agglomerated particles of the correct shape with dimensions of 100 nm or less than [7]. In this regard, the development of methods for obtaining Fe(Cr) nanopowders is an urgent task:ZnSe, and these methods themselves should have sufficiently high performance.

One of the promising methods for production of nanoparticles with the properties listed above is the method of laser synthesis, which consists in evaporation of a target of the appropriate composition using laser radiation with high average power and subsequent condensation of vapors in a buffer gas stream. The production of nanopowders of simple and complex oxides (Al_2O_3, ZrO_2, YSZ ($Y_2O_3:ZrO_2$), $Nd:Y_2O_3$, TiO_2 etc.) with a powerful continuous or repetitively-pulsed CO_2 laser [8–10], and also a continuous fiber ytterbium laser [9,11]. The production of zinc selenide nanopowders by this method has been studied much less. ZnSe nanoparticles with an average size of 16–22 nm were obtained in [12] using femtosecond Ti:sapphire laser, but due to the low average radiation power (0.8–1.3 W), the productivity was only 38 mg/h. The productivity of obtaining ZnSe nanoparticles with a continuous fiber ytterbium laser [13], generating pulsed periodic radiation with an average power of 300 W reached $\sim$ 100 g/h, and their average size was 18 nm.

It should be noted that many physical processes occur during the laser production of nanoparticles: the initial exposure of the target to the radiation, removal of matter in the form of vapor, melt drops and target fragments from the target, propagation of a laser torch into gas, formation of nanoparticles with a vapor condensation and the formation of a crystal lattice in them. In other words, the productivity of obtaining nanoparticles, their size and crystal structure depend on the properties of the material, the parameters of laser radiation and buffer gas.

A single crystal ZnSe of good quality, like many refractory oxides, has a very high transparency at the wavelength of the radiation of the ytterbium laser (1.065 nm). It is necessary to overcome the threshold of radiation destruction at the initial stage of radiation exposure to the target the evaporation of the crystal. This threshold is not overcome when oxide single crystals of oxides with good optical quality are exposed to continuous or quasi-continuous radiation from an ytterbium laser with an intensity of $I \sim 1\,\mathrm{MW/cm^2}$. However, targets with high porosity sintered from microparticles are used for producing nanopowders. In the near-surface layer of the target, the laser radiation is scattered and concentrated in some places, which contributes to the radiation destruction of the material and makes possible its further melting and evaporation [9,13]. The evaporation of refractory oxides occurs at radiation intensity $\sim 1\,\mathrm{MW/cm^2}$ by quasi-stationary evaporation of liquid melt from the crater [14], which in the case of complex oxides (YAG, $\mathrm{Nd:Y_2O_3}$ and etc.) leads to the enrichment of the obtained nanopowders with a boiling component [9,15]. It should be noted that this does not occur when the target is exposed to nanosecond or shorter radiation pulses, when the substance is removed depending on the pulse duration by explosive boiling of the melt, phase or Coulomb explosion [14].

The target vapors in the form of a laser torch are penetrate into a buffer gas after the evaporation of the target begins and they are cooled and condensed forming nanoparticles. This process takes place in a fairly short time (≈ 1 ms) and is accompanied by vortex mixing of the laser torch with buffer gas [9,16], which affects the size of the nanoparticles and the formation of their crystal lattice. However, there is little theoretical research on this topic. At the same time, there is quite a lot of experimental data on the impact of buffer gas parameters on the sizes of oxide nanoparticles obtained using a powerful CO_2 laser. It is shown in [9,17] that reduction of the pressure of the buffer gas, as well as replacement of argon or air with helium reduces the average size of Al_2O_3, ZrO_2 and $\mathrm{Nd:Y_2O_3}$ nanoparticles.

The formation of the crystal lattice of oxide nanoparticles during their laser synthesis has been studied a little better. Important factors here are also: properties of the nanoparticle material, rapid cooling of nanoparticles in the buffer gas, as well as the grade and parameters of this gas. For example, yttrium oxide nanopowders produced using a CO_2-laser or a fiber ytterbium laser form a monoclinic lattice, which is metastable [9,18,19]. Its formation was associated with a very short cooling time of steam and the resulting nanoparticles in a laser torch (≈ 1 ms), during which the steam first condenses into liquid molten nanoparticles. These nanoparticles form a monoclinic lattice after crystallization, and the stable cubic phase does not form [18]. Vaporization using a pulsed periodic CO_2-hematite laser (α-Fe_2O_3), produced nanopowders which, depending on the pressure and gas grade (Ar, air) could contain different amounts of metastable (γ-Fe_2O_3, ε-Fe_2O_3), and stable ($Fe_{3-\nu}O_4$, FeO) phases [18,20]. The formation of these phases with different oxygen content is attributable not only to the rapid cooling of nanoparticles, but also to the different behavior of oxidation-reduction reactions. At the same time, 2.7 mol.% $\mathrm{Y_2O_3:ZrO_2}$ nanopowder obtained using this laser had a tetragonal phase, and 9.85 mol.% $\mathrm{Y_2O_3:ZrO_2}$ nanopowder had a cubic lattice [21]. The same pattern as when growing single crystals of YSZ from melt appeared in this case [22].

Thus, the formation of a crystal lattice in the laser torch of nanoparticles occurs individually for each substance and largely depends on the conditions of synthesis. This is also true in the case of zinc selenide. During its evaporation in air using a femtosecond laser, ZnSe nanoparticles were obtained only in the hexagonal phase [12]. The ZnSe nanopowder already contained two crystalline phases when a continuous fiber ytterbium laser was used [13]: a stable cubic lattice of the type $F43m$ (structural type sphalerite, 40 wt.%) and a metastable hexagonal lattice of the type $P6_3mc$ (structural type wurtzite, 60 wt.%).

The purpose of this work is to study the effect of the conditions for the synthesis of zinc selenide nanoparticles using a continuous fiber ytterbium laser (grade and pressure of buffer gas, laser generation mode) on the productivity of their production, on their size and crystal structure, as well as the initial study of their pressing and sintering.

1. Description of the experimental setup and techniques

For experiments, a plant for producing nanopowders using a fiber ytterbium laser LS-9H ($\lambda = 1.06\,\mu$m, NTO „IRE Polus“) [13] was modified so that it was possible to change the pressure of the buffer gas in the evaporation chamber (Fig. 1). A target *2* was placed in the evaporation chamber *1* and a quartz lens *4* focused the laser radiation , on the surface of this target *3*. With a focal length of the lens 600 mm, the laser spot in the middle of the beam constriction had a round shape and a diameter of 650 μm. The target was rotated and moved using a special mechanism and, as it was depleted, it rose up so that its surface remained on average in the middle of the laser beam binding. The laser generated either continuous laser

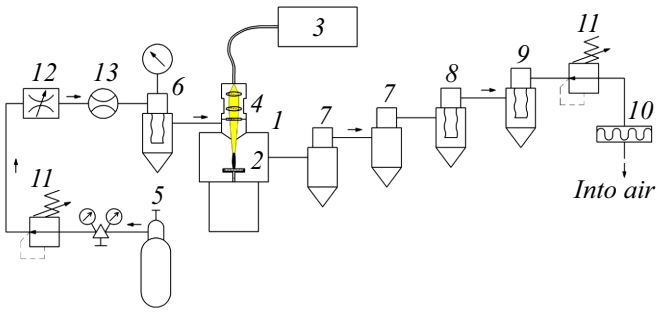

Figure 1. Block diagram of an experimental setup for producing zinc selenide nanopowders.

radiation with a power of $P_{\text{cont}} = 600$ W, or periodic rectangular radiation pulses with a duration of 120 μs and a power of $P_{\text{imp}} = 600$ W for producing nanopowder. With a pulse repetition period of 240 μs, the average radiation power in this case was 300 W. The instantaneous radiation intensity I in the laser spot was 0.18 MW/cm^2 in both modes. The nanopowder was obtained in Ar flow (purity 99.993 vol.%) or He (99.995 vol.%). The gas supplied from the cylinder *5* was pre-cleaned in the filter *6* from foreign particles and then passed through the entire plant. Laser ablation products (nanoparticles, micron drops and target fragments) together with the gas flow first fell into cyclones *7* for capturing drops and fragments of a target with a size of more than a few micrometers. The overwhelming number of nanoparticles was captured on the surface of the filter sleeve in the bag filter *8*. The material collected in this device was taken into account to calculate the productivity of obtaining nanopowder and its mass yield during evaporation of one target. Finally, the gas was released into the air after additional purification in filters *9, 10*. The absolute gas pressure in the evaporation chamber was regulated using pressure reducers *11* and throttle *12* in the range from 100 to 300 kPa. As the powder accumulated in the bag filter, the gas pressure in the chamber increased by 10–15 kPa, after which the filter was cleaned and the gas pressure decreased to the initial level. The volumetric gas flow rate was measured with a rotameter *13*.

X-ray phase analysis of the obtained nanopowders was performed on a D8 DISCOVER diffractometer in Cu radiation ($K_{\alpha_{1,2}}$, $\lambda = 1.542$ Å) using the TOPAS 3 program. The morphology of nanoparticles was studied using a transmission electron microscope JEM 2100 with a cathode of LaB_6. The specific surface area of the obtained nanopowders was measured using the TriStar 3000 V6.03A instrument according to the BET method based on the Brunauer–Emmett–Teller gas adsorption theory [23].

As a rule, ZnSe powder (qualification „H for optical ceramics“) was used for the manufacture of targets, and in one experiment, ZnSe polycrystals grown by the CVD method were used. After grinding them in a planetary ball mill with balls from WC, powders containing particles with dimensions 0.3–20 μm were obtained. The „extraction method“ [24] was used to determine the deviation of the initial ZnSe from the stoichiometric composition, which makes it possible to detect even a very small content of excess component (Zn or Se) in zinc selenide. The measurements showed that both the micro-powder and the polycrystal of zinc selenide have a fairly good degree of stoichiometry. Zinc selenide powder contained only a very small amount of excess Zn ($1.1 \cdot 10^{-7} \pm 6 \cdot 10^{-8}$ mol[Zn]/mol[ZnSe]), and polycrystal ZnSe–CVD, on the contrary, had a very small excess Se ($3.2 \cdot 10^{-7} \pm 2.4 \cdot 10^{-8}$ mol[Zn]/mol[ZnSe]). The powders obtained after grinding were pressed into compacts, which were then sintered in atmosphere H_2 at a temperature of 930°C for 6 h. The prepared targets had a density of $\approx 70\%$ of the theoretical density of zinc selenide and consisted of grains baked to each other. Micropowders of iron selenide (qualification „HC“) or copper (qualification „H“) were also used to obtain Fe:ZnSe and Cu:ZnSe nanopowders. Their chemical composition was determined using Optima 2100 spectrometer by the emission-spectral method with inductively coupled plasma (ICP-AES) with a relative measurement accuracy of 1–3% and corresponded to $FeSe_{1.03}$ and $Cu_{1.76}Se$. Mechanical mixtures of powders of simple selenides, taken in the required proportion in this case, were prepared for the manufacture of targets, which were mixed using a mixer with an inclined axis of rotation of the type „drunk barrel“ during 24 h.

2. Production of zinc selenide nanopowders with laser

The impact of the grade (Ar, He) and the pressure of an inert gas on the production of zinc selenide nanoparticles on their size and crystal structure was studied during the experiments. Based on our experience, the buffer gas parameters and the generation mode of the ytterbium laser were chosen so that the obtained zinc selenide nanopowders had the most different properties. At the same time, the impact of synthesis conditions on the productivity of nanopowder production and its mass yield was studied, which also provides understanding of the physical processes of evaporation of ZnSe.

Table 1 lists the data on the productivity of obtaining ZnSe nanopowder and its mass yield during evaporation of targets of approximately the same mass (190–200 g) under various conditions. The largest mass yield of the nanopowder (26–34% of target weight) was realized in the case of evaporation of the target by periodic radiation pulses with a duration of 120 μs in Ar or He atmospheric pressure. This was expected, since with such a duration of exposure to radiation from the crater formed in the target, the spraying of a large number of melt drops with dimensions of tens of micrometers [13] does not have time to begin. Therefore, too deep craters do not form in the target, and after repeated evaporation, its surface remains relatively flat (Fig. 2, *a*). This made it possible in this case to vaporize the target in a fairly complete way. It should be noted that the mass yield of the nanopowder turned out to be approximately the same as during evaporation of a target of the same size from $Nd:Y_2O_3$ [9]. However, the productivity of obtaining zinc selenide nanopowders (≈ 100 g/h) turned out to be 6 times greater than when yttrium oxide was vaporized by pulsed periodic radiation with the same average power 300 W. This is because Y_2O_3 has sufficiently high melting points (2430°C) and boiling points (4300°C) [25]. At the same time, zinc selenide is a substance with a sufficiently low melting point 1520°C, and it begins to sublimate already at a temperature of ~ 900°C [26]. It should be noted that the sublimation of ZnSe at this temperature was also observed in our

Figure 2. Photo of target residues after obtaining ZnSe nanopowders at Ar atmospheric pressure ($p = 100$ kPa, (a, b)) and overpressure ($p = 300$ kPa, (c)). Laser radiation generation mode — repetitively-pulsed (a) and continuous (b, c).

Table 1. Data on the productivity of obtaining nanopowders and their mass yield during evaporation of one target, as well as on the specific surface area of the obtained nanopowders depending on the conditions of evaporation of the ZnSe target using an ytterbium laser

№	Production Conditions ZnSe nanopowder	Performance Production of nanopowder, g/h	Mass Yield nanopowder, wt.%	Specific Surface Area nanopowder, m^2/g
1	Ar, $p = 100$ kPa, pulse-periodic radiation	100	34	47
2	Ar, $p = 100$ kPa, continuous radiation	190	24	38
3	Ar, $p = 300$ kPa, continuous radiation	77–82	20–21	16–18
4	He, $p = 100$ kPa, pulse-periodic radiation	95	26	66

experiments on sintering pressed zinc selenide nanopowders in an atmosphere of H_2. When the target was vaporized by continuous radiation, the nanopowder production capacity increased almost 2 times (up to 190 g/h), since the radiation power (600 W) was two times higher than the average power of pulsed periodic radiation. However, much more drops with sizes larger than $10\,\mu$m [13] are sprayed when the target is vaporized by continuous radiation, and the target surface becomes more uneven after repeated evaporation (Fig. 2, *a, b*). The maximum depth of irregularities on the target was ~ 5 mm in this case, and the depth was only ~ 2.5 mm in repetitively-pulsed laser operation. Therefore, the evaporation of the target using continuous radiation has to be stopped earlier than in the case of pulsed periodic radiation. This was the reason for the decrease of the mass yield of nanopowder from 34 to 24 wt.%.

An increase of the pressure Ar in the evaporation chamber from 100 to 300 kPa during evaporation of the target using continuous laser radiation led to a decrease of both the productivity of obtaining nanopowder and its mass yield to the minimum values in these experiments ~ 80 g/h and 21 wt.% respectively. At the same time, the maximum depth between the irregularities increased to 6 mm, and the irregularities themselves had the form of frequent needle-like protrusions (Fig. 2, *c*). The formation of a similar needle-like relief on the target was observed earlier by us during the evaporation of $Nd:Y_2O_3$ [19]. A comparison of these facts may indirectly indicate that an increase of the pressure of the buffer gas causes an increase of the splashing of the melt from the crater. However, additional, more detailed studies are required on how the grade and pressure of the buffer gas affect the dynamics of melt splashing during laser radiation exposure to zinc selenide. The impact of the grade and pressure of the buffer gas on the productivity of obtaining zinc selenide nanopowder will be discussed qualitatively below.

Photos of ZnSe nanoparticles obtained at Ar and He atmospheric pressure using the repetitively-pulsed radiation mode are shown in Fig. 3, *a, b*, and their distribution functions by size — in Fig. 3, *c*. Weak agglomeration of particles in both nanopowders is clearly visible, which is characteristic of this method of nanopowder synthesis. The nanoparticles obtained in Ar, as a rule, have the form of regular and irregular polyhedra (Fig. 3, *a*), their size distribution function has a lognormal shape. The average arithmetic size of the nanoparticles was 18 nm in this case. When the target evaporates in helium, particles are most often spherical in shape, but individual large particles are still polyhedra. The size distribution function of these nanoparticles was shifted towards smaller sizes, respectively, their average size decreased to 11 nm. The results of measurements of the specific surface area of the obtained nanopowders correlate with these data (Table 1). Its value is $66\,m^2/g$ for a nanopowder synthesized in helium, which

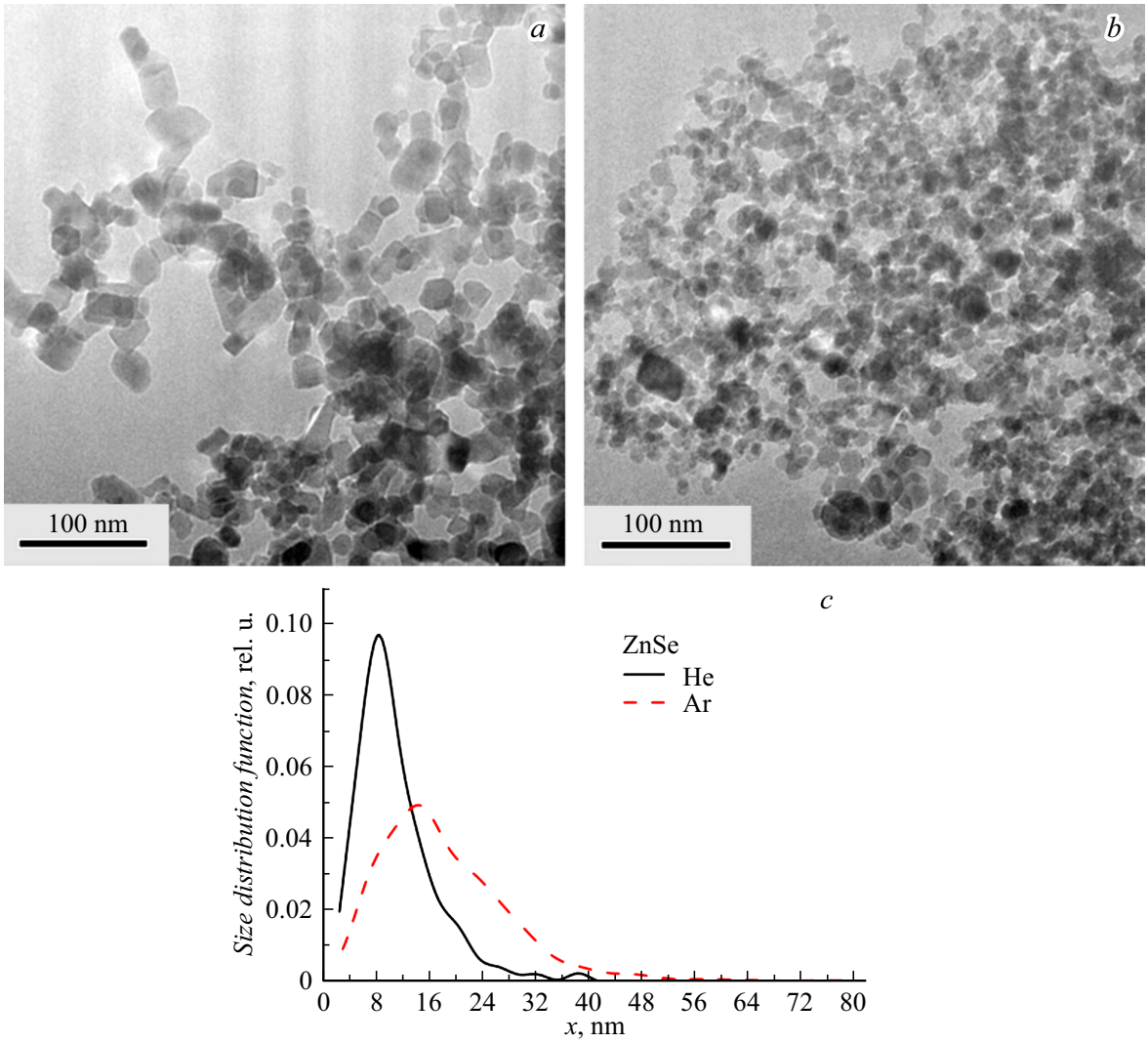

Figure 3. Photos of ZnSe nanoparticles obtained in Ar (*a*) and He (*b*) atmospheric pressure, as well as their distribution by size (*c*). Laser radiation generation mode — repetitively-pulsed.

is 1.4 times greater than that of a nanopowder obtained in argon. The transition from repetitively-pulsed to continuous evaporation of the target in the atmosphere of Ar, on the contrary, led to a certain decrease of the specific surface area of the resulting nanopowder, which indicates an increase of the size of nanoparticles. Under the same laser operation mode, an increase of argon pressure in the evaporation chamber from 100 to 300 kPa led to a further twofold decrease of the specific surface area of the nanopowder (up to 18,m^2/g), which indicates an increase of the average size of nanoparticles by about 2 times. Nanopowder with larger particles will adsorb less volatile substances from atmospheric air, including oxygen, which may be important in the manufacture of transparent ceramics from ZnSe [2].

The change of the sizes of ZnSe nanoparticles obtained under different conditions can only be explained by the fact that the buffer gas limits the spread of the laser torch and thereby affects the cooling of steam and the formation of nanoparticles. In fact, the gas controls the maximum volume of the laser torch, i.e. the concentration of steam in the condensation zone. Helium is a much lighter and more thermally conductive gas compared to argon, it restricts the spread of the laser torch less and contributes better to the cooling of steam. Therefore, the laser torch propagating into helium visually had a larger volume than when flying into argon of the same pressure. Accordingly, at a comparable evaporation rate of the target in these gases, the vapor concentration in the laser torch during its expansion into helium turns out to be less. For this reason, the nanoparticles obtained in helium have smaller sizes than in the case of argon. An increase of the buffer gas pressure leads to a decrease of the size of the laser torch and to an increase of the pressure and vapor concentration in it. At the same time, the steam flow back to the target increases, i.e. the saturated steam pressure increases. This explains why an increase of argon pressure from 100 to 300 kPa led

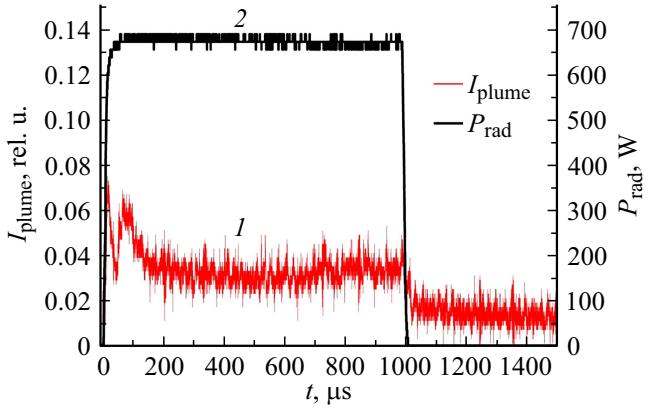

Figure 4. Waveforms of the shape of a laser pulse with an intensity on the target of ZnSe 0.46 MW/cm^2 (curve *2*) and the glow generated by its evaporation of a laser torch (curve *1*) [13].

to a decrease of the specific surface area of the resulting ZnSe nanopowder in ~ 2 times and to a certain decrease of productivity (Table 1). On the contrary, the transition from a continuous evaporation mode of the target to a pulse-periodic one led to a certain increase of the specific surface area of the ZnSe nanoparticles. This is probably caused by the fact that when the target is vaporized by radiation pulses, steam enters the condensation zone in portions, and nanoparticles do not have the opportunity to grow to large sizes.

The above arguments do not take into account the vortex-like mixing of steam in a laser torch with a buffer gas, which accelerates the formation and cooling of nanoparticles. The formation of vortices was previously detected during shadow shooting of the target evaporation process from YSZ ($Y_2O_3:ZrO_2$) in air when exposed to a pulse of CO_2 laser [16]. In our opinion, the theoretical estimate of the average size of the YSZ nanoparticles formed under these conditions, made in work [18,21], was approximately 5 times larger than the experimentally determined value because of the failure to take into account the vortex-like mixing of the laser torch with air that caused. The dynamics of the glow of a laser torch formed by evaporation of a target from ZnSe in air using a pulse of fiber laser radiation ($I = 0.46$ MW/cm^2) was studied in [13]. The oscillograms of the glow of a laser torch (curve *1*) of a laser pulse (curve *2*) are shown in Fig. 4. At the back edge of the radiation pulse, the brightness of the glow of the laser torch decreases sharply, and after the end of the laser pulse, the afterglow of the torch quickly disappears. Of course, the glow of the laser torch in this experiment can be affected by the oxidation of ZnSe with oxygen from the air. Nevertheless, it can be expected that the formation of zinc selenide nanoparticles in a laser torch occurs very quickly, within a time of no more than 1 ms. The high rate of cooling and condensation of steam, cooling of the resulting nanoparticles should not only affect the size of the nanoparticles, but also contribute to the freezing of the metastable crystal lattice. The results of experimental and theoretical studies of the influence of buffer gas parameters and the operating mode of the ytterbium laser on the crystal structure of the obtained zinc selenide nanoparticles will be presented below.

The ZnSe, Cu:ZnSe and Fe:ZnSe nanopowders obtained under various conditions using an ytterbium laser contain both a hexagonal phase of the wurtzite structural type and a cubic phase of the sphalerite structural type (Table 2, Fig. 5). When the synthesis conditions change the ratio between the contents of these phases changes, as well as the magnitude of their coherent scattering regions (CSR). At the same time, the initial ZnSe targets almost completely have a cubic crystal lattice, and the hexagonal phase is present only in the form of traces (≈ 1 wt.%). It follows from this that the formation of a metastable hexagonal lattice in zinc selenide nanopowders is associated precisely with the peculiarities of the formation of nanoparticles in a laser torch. The content of the hexagonal phase in the obtained nanopowders is 60–66 wt.%, and the rest of the powder has a cubic lattice in case of evaporation of targets from ZnSe, Cu:ZnSe and Fe:ZnSe in atmospheric pressure argon ($p = 100$ kPa) using repetitively-pulsed laser radiation. The average sizes of crystallites in these phases (CSR = 17–25 nm) coincide well with the arithmetic mean size of zinc selenide nanoparticles (18 nm), which was calculated from electron microscopy data. Upon evaporation of the ZnSe target in helium of the same pressure and at the same radiation parameters, the CSR of the cubic and hexagonal phases of the obtained nanopowders decreased to 9–11 nm, which also coincides with the average size of the nanoparticles contained in them (11 nm). The content of the metastable hexagonal phase in the ZnSe nanopowder obtained in He was 69 wt.%, which is slightly more than when the target evaporated in the atmosphere Ar. The transition from repetitively-pulsed laser radiation to continuous laser operation with the same buffer gas parameters has little changed the crystal structure of ZnSe nanoparticles. At the same time, an increase of argon pressure to $p = 300$ kPa led to an increase of the content of the hexagonal phase (up to 81–83 wt.%), and also to a significant increase of the average size of crystallites in both phases (up to 32–40 nm).

The following can be summarized discussing the results of the experiments. Since ZnSe evaporation occurs almost congruently [26], the formation of a hexagonal or cubic crystal lattice in ZnSe nanoparticles is associated only with the conditions of their formation during vapor condensation in a laser torch. The mode of generation of a fiber ytterbium laser (continuous or pulse-periodic) has little effect on the size and crystal structure of the resulting ZnSe nanoparticles. This impact is reduced to a certain increase of the size of nanoparticles in the continuous evaporation mode of the target, since the vaporized substance enters the vapor condensation zone continuously, and not in portions. To a much greater extent, the structure of nanoparticles is affected by changes in the parameters of the buffer gas, on which the dynamics of propagation

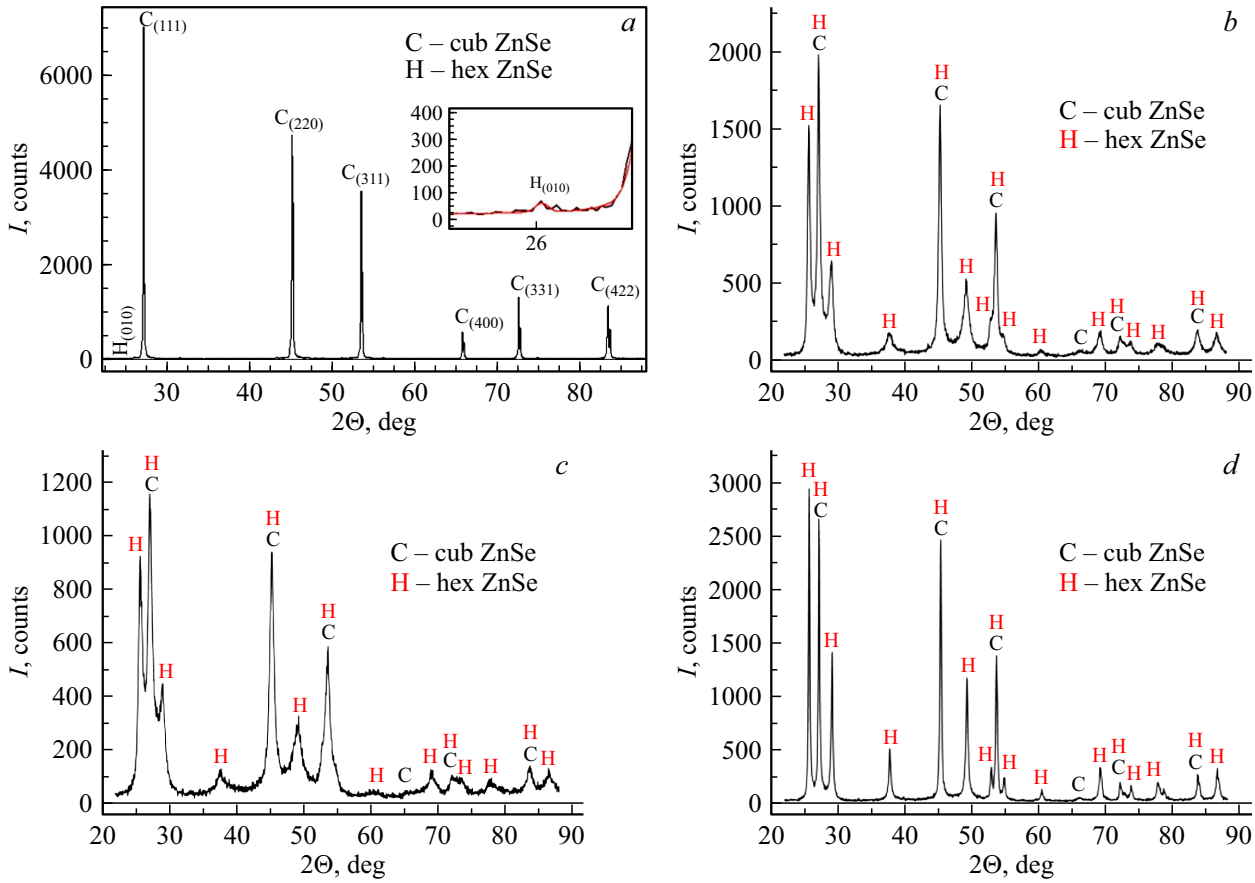

Figure 5. Radiographs of the initial target from ZnSe (*a*) and ZnSe nanopowders obtained in Ar (*b, d*) and He (*c*) at a pressure of 100 kPa (*b, c*) and 300 kPa (*d*) with repetitively-pulsed (*b, c*) and continuous (*d*) the generation mode of a fiber ytterbium laser.

and cooling of the laser torch largely depends. Helium limits the expansion of the laser torch less than argon, and due to higher thermal conductivity cools the steam faster, which accelerates the formation and cooling of nanoparticles. On the one hand, the ZnSe nanopowder obtained in helium actually contains nanoparticles with a smaller average size. On the other hand, the content of the metastable hexagonal phase in it turned out to be slightly higher than when using argon. At the same time, an increase of Ar pressure leads to an increase of the vapor concentration of the laser torch and the size of the resulting nanoparticles. It is possible to expect that this would decrease the cooling rate of the laser torch and, accordingly, the content of the hexagonal phase in the nanopowder. However, an increase of pressure Ar from 100 to 300 kPa, on the contrary, led to an increase of the content of the hexagonal phase from 66 to $\sim$ 80 wt.% according to experimental data. This contradiction indicates a more complex nature of the processes of formation of nanoparticles in a laser torch than it seems. For example, it is necessary to take into account the impact of the formation of vortices at the boundary of the laser torch, which accelerates the cooling of steam in the laser torch and the formation of nanoparticles. It is possible that some other factor also impacts the formation of the crystal lattice of nanoparticles.

In the above reasoning, by analogy with the work [18] the following sequence of formation of crystalline nanoparticles in a laser torch was assumed. The steam propagating into the buffer gas is rapidly supercooled, which leads to the formation of condensation centers — nuclei of future nanoparticles. The nanoparticles formed in this way are initially in a molten state, and their crystallization occurs when they cool down further. In this case, a high-temperature, metastable crystal lattice is first formed, which in the case of Y_2O_3 is monoclinic, and in the case of ZnSe — hexagonal. A stable lattice can be formed by further cooling of nanoparticles as a result of a polymorphic phase transition. However, due to the rapid cooling of nanoparticles in the laser torch and in the gas, such a phase transition may not have time to occur. This is exactly what happens when obtaining nanoparticles Y_2O_3, in which „freezes“ monoclinic phase [18,19]. The presence of metastable (hexagonal) and stable (cubic) phases in the ZnSe nanopowder at once could be explained by analogy by the incompleteness of the polymorphic phase transition. The characteristic transformation time of a hexagonal ZnSe lattice into a cubic lattice was theoretically estimated.

Table 2. Results of X-ray phase analysis of targets from ZnSe and ZnSe, Cu : ZnSe and Fe : ZnSe nanopowders obtained under different conditions

Sample (conditions for obtaining)	Cubic ZnSe (F-43m, PDF № 00-037-1463, a=5.6688 Å)			Hexagonal ZnSe ($P6_3mc$, PDF № 01-089-2940, a=3.996 Å, c=6.626 Å)		
	Parameters lattices, Å	OKP, nm	Contents, wt.%	Parameters lattices, Å	OKP, nm	Contents, wt.%
Target ZnSe	$a = 5.6696$	> 200	≈ 99	$a = 3.95$, $c = 6.64$	–	≈ 1
Target ZnSe (from ZnSe-CVD)	$a = 5.670$	> 200	100	–	–	–
Nanopowder ZnSe (Ar, 100 kPa, pulse-periodic)	$a = 5.669$	21	40	$a = 3.999$, $c = 6.579$	17	60
Nanopowder Cu:ZnSe (Ar, 100 kPa, pulse-periodic)	$a = 5.669$	24	34	$a = 3.998$, $c = 6.578$	18	66
Nanopowder Fe:ZnSe (Ar, 100 kPa, pulse-periodic)	$a = 5.670$	22	34	$a = 4.001$, $c = 6.578$	18	66
Nanopowder ZnSe (He, 100 kPa, pulse-periodic)	$a = 5.672$	9	31	$a = 4.003$, $c = 6.588$	11	69
Nanopowder ZnSe (Ar, 100 kPa, continuous)	$a = 5.669$	23	34	$a = 4.001$, $c = 6.578$	18	66
Nanopowder ZnSe (Ar, 300 kPa, continuous)	$a = 5.670$	40	19	$a = 4.003$, $c = 6.572$	38	81
Nanopowder ZnSe (from ZnSe-CVD, Ar, 300 kPa, continuous)	$a = 5.668$	32	17	$a = 4.002$, $c = 6.571$	40	83

To calculate the transition of ZnSe nanoparticles from the hexagonal phase to the cubic one, a technique developed by us earlier in work [27] was used. The characteristic transition time was calculated using the following formula

$$\tau = \left(A\sqrt{kT}\exp\left(-\frac{Q}{kT}\right)\right)^{-1}, \qquad (1)$$

where T — temperature, k — Boltzmann constant, A — proportionality coefficient, Q — activation energy of the phase transition.

Special experiments were carried out on calcination of ZnSe nanopowder in a hydrogen atmosphere at different temperatures for 4 h with heating and cooling rate 3°C/min to determine the magnitude of the proportionality coefficient A and the activation energy of the phase transition Q. A nanopowder poured into a corundum boat for calcination without any pre-pressing that was obtained in Ar ($p = 100$ kPa) by vaporization of the target by pulsed-periodic laser radiation was used for this purpose. In other words, the same nanoparticles that were formed in the laser torch were subjected to temperature treatment. The data on the content of the cubic phase in nanopowders calcined at different temperatures are given in fig. 6, *a*.

A formula for calculating the concentration of the cubic phase in calcined nanopowders can be obtained using the expression (1):

$$\delta_c = 1 - \delta_h = 1 - \delta_{h0}\exp\left(-\int A\sqrt{kT(t)}\exp\left(-\frac{Q}{kT(t)}\right)dt\right), \qquad (2)$$

where δ_c and δ_h — fractions, respectively, of the cubic and hexagonal phase after annealing, δ_{h0} — fraction of the hexagonal phase before annealing.

Integration in the formula (2) was carried out over the entire calcination cyclogram implemented in the experiment. The initial content of the cubic phase in the nanopowder was assumed to be 40 wt.% during calculations. Comparison of experimental and calculated data made it possible to find the values of the desired parameters: $A = 2.15 \cdot 10^{13}\,\mathrm{J}^{-1/2}/\mathrm{s}$, $Q = 1.5$ eV. The calculated and experimental dependences of the cubic phase content in nanopowders on the calcination temperature within the measurement error coincide well (Fig. 6, *a*), which indicates the adequacy of the overall

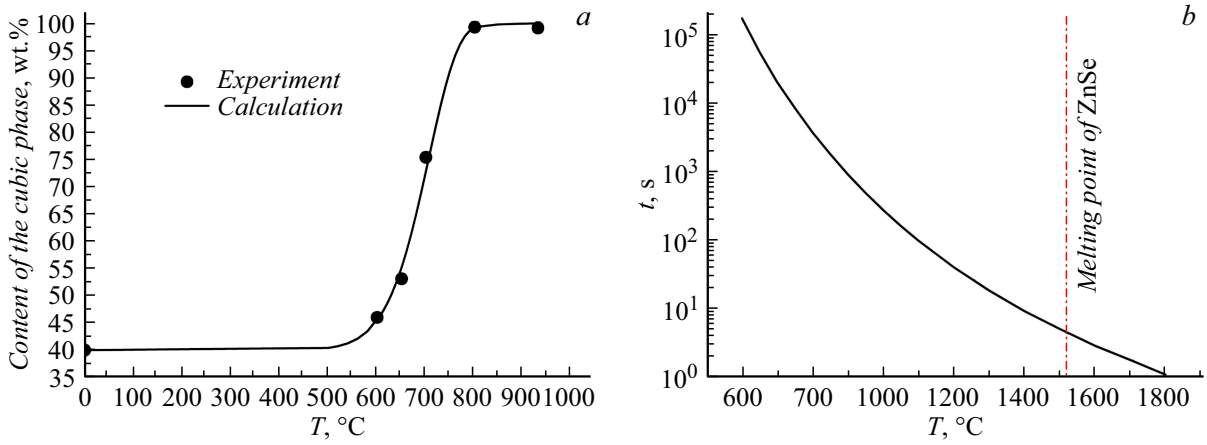

Figure 6. Cubic phase content in ZnSe nanopowder after its calcination at different temperatures for 4 h and heating and cooling rates 3°C/min ((*a*), experiment and calculation), and the calculated dependence on the temperature of the characteristic time of the phase transition from the hexagonal phase to the cubic (*b*).

model of the phase transition during calcination of ZnSe nanopowder obtained by laser. It is noteworthy that the hexagonal phase completely turns into a cubic one at the calcination temperature of ≈ 900°C. This temperature turned out to be significantly lower than the temperature of this phase transition (≈ 1410°C) for massive ZnSe samples grown from the melt [28] or by the CVD [29] method. Such a significant difference in phase transition temperatures for ZnSe nanoparticles and ZnSe bulk material can be explained by the fact that nanoparticles have a higher surface energy. Accordingly, the activation energy and the phase transition temperature of ZnSe nanoparticles turns out to be less than that of the bulk material.

The model described above was used to estimate the characteristic time required for the formation of a cubic phase in nanoparticles in a laser flare, initially having a hexagonal lattice. The dependence of this time on the temperature of nanoparticles calculated using formula (1) is shown on fig. 6, *b*. We do not have specific data on what the maximum temperature of vapor and nanoparticles is realized in a laser torch. It is obvious that at the moment of crystallization, the temperature of the nanoparticles cannot exceed the melting point of ZnSe ($T = 1520$°C). However, even at such a temperature, the estimated time of the phase transformation of a hexagonal lattice into a cubic lattice is ~ 5 s, and as the temperature decreases, it increases exponentially. This is several orders of magnitude longer than the experimentally measured decay time of the laser flare after the end of the laser pulse ($\sim 200\,\mu$s). In any case, the residence time of nanoparticles in the hot zone of the laser torch is unlikely to exceed the value of ~ 1 ms, which is also clearly insufficient for the phase transition. At the same time, a significant proportion of the obtained ZnSe nanopowder (19–40 wt.%) has a cubic lattice according to the analysis data. This implies the obvious inaccuracy of the assumption that the molten ZnSe nanoparticles formed in the laser torch after crystallization first have a hexagonal phase, which, when they cool down, turns into a cubic phase. It is logical to assume the following. If zinc selenide begins to sublimate already at a temperature of ~ 900°C when the target is heated by laser radiation, then vapor condensation from Zn atoms and Se_2 molecules can at least partially occur by desublimation with the formation of solid nanoparticles at once, which form either cubic, or a hexagonal lattice. The content of these phases in ZnSe nanopowders obtained by laser should correlate with the statistics of their formation in solid nuclei of nanoparticles.

It is necessary to emphasize once again that nanoparticles are formed quickly within maximum 1 ms. For this reason, some nanoparticles may have various defects in the crystal structure. For example, it was noted in [30] that ZnSe nanoparticles obtained using a fiber ytterbium laser had structural defects of the type of crystallographic shift (Magneli phases and Wadsley defects), and many nanoparticles with sizes less than 5 nm had an amorphous structure. Since steam desublimation, formation and cooling of nanoparticles occur under conditions of vortex mixing of a laser torch with a buffer gas, these processes should depend on the parameters of the buffer gas flow. The change in the conditions of synthesis of ZnSe nanopowders in the experiment, indeed, leads to a certain change in the content of cubic and hexagonal phases in them. It is clear that the formation of ZnSe nanoparticles during the propagation of a laser torch into a buffer gas is quite complex and requires further investigation.

3. Pressing and sintering of zinc selenide nanopowders

Initial studies of the compaction of the obtained zinc selenide nanopowders and their further sintering were carried out in this paper. For this purpose, ZnSe, Cu : ZnSe, Fe : ZnSe nanopowders synthesized under atmospheric pressure by evaporation of the target by repetitively-pulsed laser

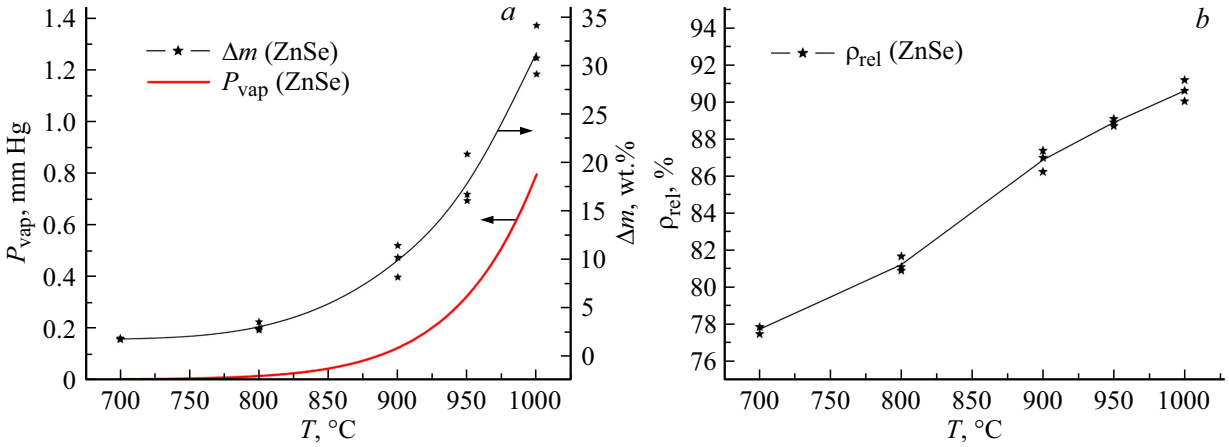

Figure 7. The dependence of the saturated vapor pressure ZnSe (P_{vap}) and mass removal (Δm) of ZnSe nanopowder compacts during their sintering in a hydrogen atmosphere on temperature (a), and also the dependence of the relative densities (ρ_{rel}) of ZnSe ceramics made of nanopowders on their sintering temperature (b).

radiation were used. The nanopowders were pressed using a uniaxial hydraulic press at a pressure of 133 MPa, as well as by magnetic pulse pressing (MPP) [31]. In the case of MPP, the nanopowder is compacted in a collapsible mold with a channel diameter of 15 mm. After filling into the mold, the nanopowder was not additionally pressed so that its degassing before pressing took place more intensively, which had a positive effect on the final density of the compressed sample. Degassing was performed at temperatures of 300 and 430°C and vacuuming to residual pressure ~ 10 Pa. After that, nanoparticle magnetic pulse pressing was carried out using a concentrator accelerated in a magnetic field, which shocklessly affects the punch for a short time (300–500 μs) and at high pressure (of the order of 1 GPa), which made it possible to achieve a significantly higher compact density than when using uniaxial hydraulic press.

The loss of the mass of ZnSe compacts during sintering in the atmosphere H_2 during 2 h at different temperatures was studied at the first stage. For this purpose, compacts with a diameter of 15 mm and a thickness of 2.4–2.6 mm with a relative density of 49–54% of the theoretical density of ZnSe were used using a uniaxial press. It was found that during sintering they lost a lot of mass, and the mass loss increased non-linearly from ~ 2 to 30–35 wt.% with an increase of the sintering temperature from 700 to 1000°C (Fig. 7, a). The course of this curve qualitatively repeats the temperature dependence of the saturated vapor pressure over solid ZnSe under vacuum conditions on the temperature, which was calculated using the following formula [26]:

$$\lg(p_{\text{over solid}}\,[\text{mm Hg}]) = 9.436 + \frac{12140}{T[^\circ\text{C}] + 273},$$

where

$$T = 679 - 936^\circ\text{C}. \qquad (3)$$

A comparison of these data suggests that the decrease of the mass of samples from pressed zinc selenide nanopowder during their sintering is attributable to the evaporation of this material, which should be taken into account when developing the technology for producing transparent ceramics.

The compaction of compacts during their sintering depending on the method of compacting the nanopowder, temperature and sintering time was further studied. Fig. 7, b shows the results of sintering of ZnSe compacts obtained using a hydraulic press and having a density of 49–54% of the theoretical density of a single crystal. After sintering for 2 h at a temperature of 700°C, the relative density of compacts increased to 78%, and with an increase of the sintering temperature to 1000°C, it increased to ~ 90%.

Compacts obtained by magnetic pulse pressing of ZnSe, Cu:ZnSe, Fe:ZnSe nanopowders with comparable sizes had a much higher density than in the case of uniaxial static pressing. These samples were sintered at a temperature of 950°C for 2 or 3 h. Ceramics with a relative density of up to 99% were made from compacts that originally had a density of 66–74% (Fig. 8), which, however, were not transparent. Interestingly, compacts with a relative density of 91%, practically did not shrink during sintering: the density of sintered ceramics was only 92% of the theoretical density. In addition, compacts with such a high relative density during sintering often cracked due to too high mechanical stresses that occur during magnetic pulse pressing. Thus, the initial density of compacts is the most important parameter on which the dynamics of the sintering process of the pressed nanopowder depends. The relative density of compact ~ 70% seems to be optimal for manufacturing ceramics by this method.

In general, it should be noted that in order to obtain transparent ceramics from zinc selenide, it is necessary to conduct additional studies of nanopowder pressing and its further sintering.

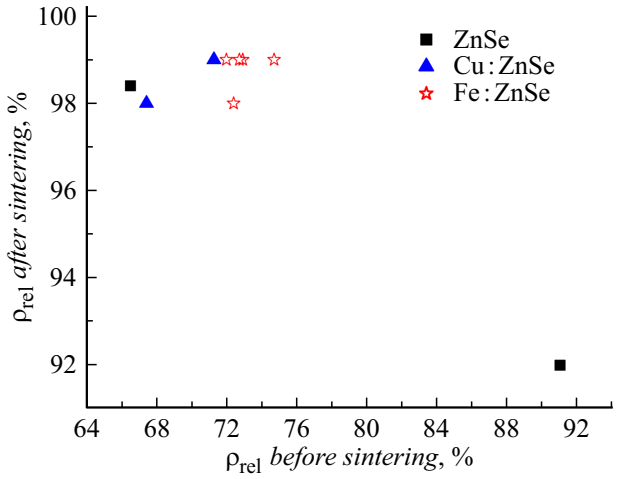

Figure 8. Relative density of ceramics ZnSe, Cu : ZnSe, Fe : ZnSe depending on the relative density of the initial compacts from the corresponding nanopowders obtained using laser. Ceramics was sintered at a temperature of 950°C for 2 (ZnSe and Cu : ZnSe) and 3 h (Fe : ZnSe).

Conclusion

The results of the performed studies on the production of weakly agglomerated zinc selenide nanopowders using a fiber ytterbium laser and experiments on their pressing and sintering allow drawing the following conclusions.

1. The average size of the obtained zinc selenide nanoparticles primarily depends on the pressure and grade (Ar, He) of the buffer gas, which, by limiting the propagation of the laser torch, affects the dynamics of vapor and the formation of nanoparticles. For example, when the target was vaporized by periodic laser pulses with a duration of 120 μs, the replacement of Ar with a lighter and thermally conductive He of the same pressure ($p \approx 100$ kPa) led to a decrease of the average size of nanoparticles from 18 to 11 nm. An increase of pressure Ar to $p = 300$ kPa, on the contrary, led to an increase of the average size of nanoparticles in ~ 2 times. The transition from the pulse-periodic mode of laser radiation to the continuous mode also led to a certain increase of the size of nanoparticles.

2. The productivity of obtaining ZnSe nanopowders and its mass yield during evaporation of one target depends on the parameters of laser radiation and buffer gas. The highest productivity of obtaining nanopowder (190 g/h) was realized when ZnSe was evaporated in an atmosphere of Ar of normal pressure ($p \approx 100$ kPa) by continuous radiation with a power of 600 W. Evaporation of the target by periodic pulses with a duration of $t_{imp} = 120\,\mu$s and with the same power (600 W) made it possible to reduce the splashing of melt drops and increase the yield of nanopowder to ~ 30 wt.%, however, due to a decrease of the average radiation power to 300 W the nanopowder production capacity decreased to 100 g/h. An increase of pressure Ar to 300 kPa led to a decrease of the productivity of obtaining nanopowder under continuous laser operation from 190 to 80 g/h, which is explained by an increase of the pressure of saturated zinc selenide vapors in the laser torch.

3. The resulting ZnSe nanopowders contain both a stable cubic crystal lattice (structural type sphalerite) and a metastable hexagonal lattice (structural type wurtzite). The CSR value of these phases coincides well with the arithmetic mean size of the nanoparticles. The content of the cubic phase in the nanopowder, depending on the pressure ($p = 100-300$ kPa) and the grade (Ar or He) of the buffer gas, varies within 17–40 wt.%.

4. From the totality of theoretical and experimental data, it follows that many or all ZnSe nanoparticles are formed in a laser torch by desublimation of steam immediately into solid nanoparticles, and not by its condensation through the melt phase. In this case, the ratio between the content of cubic and hexagonal phases in nanopowders should reflect the statistics of their formation in the crystalline nuclei of nanoparticles.

5. The first experiments with the manufacture of ceramics from ZnSe showed that pressing of the obtained nanopowders using a uniaxial hydraulic or magnetic pulse press followed by sintering of the compacts in a hydrogen atmosphere 950°C allows obtaining only opaque ceramics with a density up to $\sim 99\%$ of the theoretical density of selenide zinc. The sublimation of ZnSe at a temperature above 900°C is one of the most important factors to be taken into account when developing the technology for manufacturing transparent ceramics.

Acknowledgments

The authors would like to thank Cand. Phys.-Math.Sci. A.M. Murzakaeva and junior research associate O.R. Timoshenkov for photographing nanoparticles using a transmission electron microscope, Cand. Sc. Chemistry D.G. Lisienko (Institute of Physics and Technology UrFU) for analysis of nanopowders by ICP-AES,Cand. Sc. Chemistry A.V. Abramova (Institute of Physics and Technology UrFU) and V.A. Shitova (IEP UB RAS) for assistance in the fabrication of targets for evaporation. Photographing of nanoparticles, X-ray phase analysis and specific surface area analysis were carried out on the equipment of the Institute of Electrophysics of the Ural Branch of RAS.

Funding

This work was funded by the Russian Science Foundation and the Government of the Sverdlovsk region (grant No. 22-29-20039, https://rscf.ru/project/22-29-20039/).

Conflict of interest

The authors declare that they have no conflict of interest.

References

[1] N.A. Kulchitsky, A.V. Naumov, V.V. Startsev. Uspekhi prikladnoi fiziki, **7** (4), 374 (2019) (in Russian).

[2] E.M. Gavrushchuk. Inorganic Mater., **39** (9), 883 (2003). DOI: 10.1023/A:1025529017192

[3] S.D. Velikanov, N.A. Zaretsky, A.V. Zakhryapa, A.A. Maneshkin, E.V. Saltykov, R.S. Chuvatkin, I.M. Yutkin, E.M. Gavrishchuk, V.B. Ikonnikov, S.Yu. Kazantsev, I.G. Kononov, D.A. Mashkovskii, K.N. Firsov. Quant. Electron., **47** (4), 303 (2017). DOI: 10.1070/QEL16324

[4] V.I. Kozlovsky, Y.V. Korostelin, Y.P. Podmar'kov, Y.K. Skasyrsky, M.P. Frolov. J. Phys.: Conf. Series, **740**, 012006 (2016). DOI: 10.1088/1742-6596/740/1/012006

[5] I. Moskalev, S. Mirov, M. Mirov, S. Vasilyev, V. Smolski, A. Zakrevskiy, V. Gapontsev. Optics Express, **24** (18), 21090 (2016). DOI: 10.1088/1742-6596/740/1/012006

[6] K. Karki, Sh. Yu, V. Fedorov, D. Martyshkin, Sh. Subedi, Y. Wu, S. Mirov. Opt. Mater. Express, **10** (12), 3417 (2020). DOI: 10.1364/OME.410941

[7] S.G. Garanin, N.N. Rukavishnikov, A.V. Dmitryuk, A.A. Zhilin, M.D. Mikhălov. J. Opt. Technol., **77** (9), 565 (2010). DOI: 10.1364/JOT.77.000565

[8] H.-D. Kurland, J. Grabow, F.A. Müller. J. Europ. Ceramic Society, **31** (14), 2559 (2011). DOI: 10.1016/j.jeurceramsoc.2011.01.010

[9] V.V. Osipov, V.V. Platonov, V.V. Lisenkov, E.V. Tikhonov. Inorganic Mater.: Appl. Res., **13** (3), 674 (2022). DOI: 10.1134/S2075113322030285

[10] M. Kato. Jpn. J. Appl. Phys., **15** (5), 757 (1976). DOI: 10.1143/JJAP.15.757

[11] Y.A. Kotov, O.M. Samatov, M.G. Ivanov, A.M. Murzakaev, A.I. Medvedev, O.R. Timoshenkova, T.M. Demina, I.V. V'yukhina. Tech. Phys., **56** (5), 652 (2011). DOI: 10.1134/S1063784211050173

[12] H.I. Wang, W.T. Tang, L.W. Liao, P.Sh. Tseng, Ch.W. Luo, Ch.Sh. Yang, T. Kobayashi. J. Nanomater., **2012**, ID 278364 (2012). DOI: 10.1155/2012/278364

[13] V.V. Osipov, V.V. Platonov, A.M. Murzakaev, E.V. Tikhonov, A.I. Medvedev. Bulletin of the Lebedev Physics Institute, **49** (Supplement Issue 1), S78 (2022) DOI: 10.3103/S1068335622130085

[14] A.V. Bulgakov, N.M. Bulgakova, I.M. Burakov, N.Y. Bykov, A.N. Volkov, B.J. Garrison, K. Guri, L.V. Zhigilev, D.S. Ivanov, T.E. Itina, N.I. Kuskova, M. Kjellberg, E.E.B. Campbell, P.R. Levashov, E. Levegl, J. Lin, G.A. Lukyanov, V. Marin, I. Ozerov, A.E. Skew, M.E. Povarnitsyn, A.D. Rud, V.S. Sedoy, K. Hansen, M. Heden, K.V. Predatenko. *Sintez nanorazmernyh materialov pri vozdejstvii moshchnyh potokov energii na veshchestvo* (Institut teplofiziki SO RAN, Novosibirsk, Novosibirsk, 2009)

[15] V.V. Osipov, V.V. Lisenkov, V.V. Platonov. Tech. Phys. Lett., **37** (1), 49 (2011).

[16] V.V. Osipov, V.V. Platonov, V.V. Lisenkov. Quant. Electron., **39** (6), 541 (2009). DOI: 10.1070/QE2009v039n06ABEH013981

[17] V.N. Snytnikov, Vl.N. Snytnikov, D.A. Dubov, V.I. Zaikovskii, A.S. Ivanova, V.O. Stoyanovskii, V.N. Parmon. J. Appl. Mechan. Tech. Phys., **48** (2), 292 (2007). DOI: 10.1007/s10808-007-0038-3

[18] V.V. Osipov, V.V. Platonov, V.V. Lisenkov. In: *Handbook of Nanoparticles,* Vol. 2), ed. by M. Aliofkhazraei (Springer International Publishing, Switzerland, 2015), p. 1. DOI: 10.1007/978-3-319-13188-7_8-1

[19] V.V. Osipov, V.V. Platonov, V.V. Lisenkov, E.V. Tikhonov, A.V. Podkin. Appl. Phys. A, **124**, Article number 3 (2018). DOI: 10.1007/s00339-017-1348-9

[20] V.V. Osipov, V.V. Platonov, M.A. Uimin, A.V. Podkin. Tech. Phys., **57** (4), 543 (2012).

[21] V.V. Osipov, Yu.A. Kotov, M.G. Ivanov, O.M. Samatov, V.V. Lisenkov, V.V. Platonov, A.M. Murzakaev, A.I. Medvedev, E.I. Azarkevich. Laser Phys., **16** (1), 116 (2006). DOI: 10.1134/S1054660X06010105

[22] Yu.S. Kuzminov, V.V. Osiko. *Fianity. Osnovy tekhnologii, svojstva, primenenie* (Nauka, M., 2001)

[23] A.P. Karnaukhov. *Tekstura dispersnyh i poristyh materialov* (Nauka. Sib. enterprise RAS, Novosibirsk, 1999)

[24] I. Avetissov, E. Mozhevitina, A. Khomyakov, T. Khanh. Crystal Res. Technol., **50** (1), 93 (2015). DOI: 10.1002/crat.201400201

[25] A.P. Babichev, N.A. Babushkina, A.M. Bratkovsky, M.E. Brodov, M.V. Bystrov, B.V. Vinogradov, L.I. Vinokurova, E.B. Gelman, A.P. Geppe, I.S. Grigoryev, K.G. Gurtovoy, V.S. Egorov, A.V. Eletsky, L.K. Zarembo, V.Y. Ivanov, V.L. Ivashintseva, V.V. Ignatiev, R.M. Imamov, A.V. Inyushkin, N.V. Kadobnova, I.I. Karasik, K.A. Kikoin, V.A. Krivoruchko, V.M. Kulakov, S.D. Lazarev, T.M. Lifshits, Yu.E. Lubarsky, S.V. Marin, I.A. Maslov, E.Z. Meilikhov, A.I. Migachev, S.A. Mironov, A.L. Musatov, Yu.P. Nikitin, L.A. Novitsky, A.I. Obukhov, V.I. Ozhogin, R.V. Pisarev, Yu.V. Pisarevsky, V.S. Ptuskin, A.A. Radzig, V.P. Rudakov, B.D. Summ, R.A. Sunyaev, M.N. Khlopkin, I.N. Khlustikov, V.M. Cherepanov, A.G. Chertov, V.G. Shapiro, V.M. Shustriakov, S.S. Yakimov, V.P. Yanovsky. *Fizicheskie velichiny: Spravochnik*. Ed. by I.S. Grigor'ev, E.Z. Meilikhov (Energoatomizdat, M., 1991), p. 298 (in Russian).

[26] V.N. Volodin, S.A. Trebukhov. *Distillyacionnye processy izvlecheniya i rafinirovaniya selena* (Almaty, 2017) (in Russian).

[27] V.V. Osipov, V.I. Solomonov, V.A. Shitov, V.V. Lisenkov, A.V. Spirina, K.E. Lukyashin. Ogneupory i tekhnicheskaya keramika, **1**–**2**, 56 (2010) (in Russian).

[28] L.V. Atroschenko, S.N. Galkin, I.A. Rybalka, A.G. Fedorov, E.F. Voronkin, A.I. Lalayants, V.D. Ryzhikov. Izvestiya vuz. Materialy elektronnoy tekhniki, **2**, 60 (2006) (in Russian).

[29] H. Okada, T. Kawanaka, S. Ohmoto. J. Crystal Growth, **165** (1−2), 31 (1996). DOI: 10.1016/0022-0248(96)00166-2

[30] A.M. Murzakaev, V.V. Osipov, V.V. Platonov. Physics of the Solid State, **64** (11), 1641 (2022). DOI: 10.21883/PSS.2022.11.54185.375

[31] E.A. Olevsky, A.A. Bokov, G.Sh. Boltachev, N.B. Volkov, S.V. Zayats, A.M. Ilyina, A.A. Nozdrin, S.N. Paranin. Acta Mech., **224** (12), 3177 (2013). DOI: 10.1007/s00707-013-0939-6

Translated by Ego Translating